Impact of Payload Distortions on BeiDou B1I-B1C Meta-Signal Ranging Performance

Florian C. Beck[1,2], Christoph Enneking[1], Steffen Thölert[1,2], Michael Meurer[1,2]

[1] *Institute for Communications and Navigation, German Aerospace Center (DLR)*
[2] *Chair of Navigation, RWTH Aachen University, 52062 Aachen, Germany*

BIOGRAPHY

Florian C. Beck received the B.Sc. and M.Sc. degrees in Electrical and Computer Engineering from the Technical University of Munich, Germany, in 2017 and 2020, respectively. Since 2020, he has been an Associate Researcher with the Department of Navigation, Institute of Communications and Navigation of the German Aerospace Center (DLR), Wessling, Germany and began his doctorate studies at RWTH Aachen University in 2022. His research interests include satellite navigation performance and signal design.

Christoph Enneking received the B.Sc. and M.Sc. degrees in Electrical Engineering from the Technical University of Munich, Germany, in 2012 and 2014, respectively. He received the doctor degree (Ph.D.) in teleinformatics engineering from the Federal University of Ceara (UFC), Brazil, in 2020. In September 2014, he joined the Institute of Communications and Navigation of the German Aerospace Center (DLR), Germany. His research interests include GNSS signal design, estimation theory and GNSS intra- and intersystem interference.

Steffen Thölert received his diploma degree in electrical engineering from the University of Magdeburg in 2002. In May 2006 he joined the Institute of Communications and Navigation of the German Aerospace Center (DLR). His current research activities include signal quality monitoring, satellite payload characterization, system calibration, GNSS compatibility and interference.

Michael Meurer is the supervisor of the Navigation department of the German Aerospace Center (DLR). In addition, he is a professor of electrical engineering and director of the Chair of Navigation at the RWTH Aachen University. His current research interests include GNSS signals, GNSS receivers, and navigation for safety-critical applications.

ABSTRACT

Recently, BeiDou satellite system (BDS) added the new civil signal B1C to its signal portfolio. As its carrier frequency is offset with respect to the legacy B1I signal, the two can be tracked jointly as a meta-signal with a larger combined bandwidth and better tracking accuracy. The cross-correlation function (CCF) of such a meta-signal has a sharp main peak, but also several stable side peaks. Payload distortions, resulting from imperfect filter and power amplifier components, are known to alter the shape of the CCF, making it more likely that one false tracking point will be misidentified as the correct lock point. This study illustrates the effect of linear and non-linear payload distortions on state-of-the-art dual band tracking (DBT) and meta-signal processing (MSP) processing schemes and shows the expected ranging performance degradation for the BDS B1I+B1C meta-signal.

I. INTRODUCTION

Global navigation satellite systems (GNSS) provide a wide range of navigation signals in the lower L-band from 1164 to 1300 MHz and in the upper L-band from 1559 to 1610 MHz. The more recently added signals in the lower L-band (e.g. L5, E5a, B2a) provide better theoretical ranging capabilities due to their larger bandwidth (Betz and Kolodziejski, 2009). Currently, there is no such wideband civil signal in the upper L-band. The growing demand in the mass market and the shortcomings of the current GNSS signal landscape have fueled a discussion to fill this gap by adding additional signals that can be used not only as novel stand-alone signals, but also in combination with the legacy signals to form a broadband meta-signal (Paonni and Bavaro, 2013; Anghileri et al., 2018; Sénant et al., 2018). With the deployment of its third generation satellites, BeiDou satellite system (BDS) offers the novel B1C signal and the legacy B1I signal − both placed in the upper L-band but at different center frequencies. This provides an interesting opportunity to put the idea of meta-signal processing (MSP) to the test.

Fig. 1 illustrates the power spectral densities (PSDs) of the complete BeiDou 3rd generation B1 signal and the B1I and B1C signals with their center frequency placed at $f_{0,\mathrm{B1I}} = 1561.098$ MHz and $f_{0,\mathrm{B1C}} = 1575.420$ MHz respectively (China Satellite Navigation Office, 2019, 2017) resulting in a 14.322 MHz frequency offset. Fig. 2 shows the auto-correlation functions (ACFs) of the B1I and B1C signal and the multi-peaked ACF of B1I+B1C meta-signal at their carrier frequencies assuming a power ratio of of $4:3$ between the B1I and B1C signals.

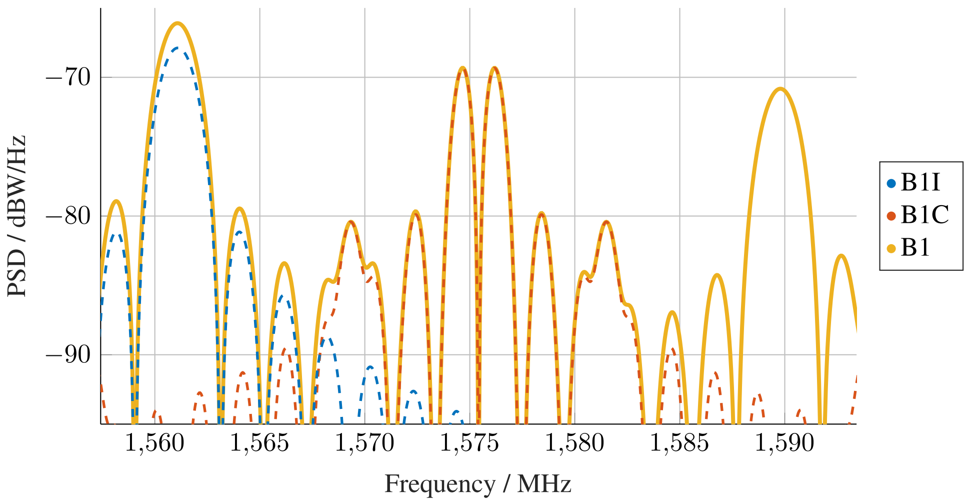

Figure 1: *Power-Spectral Densities of BDS-3 B1 Signals*

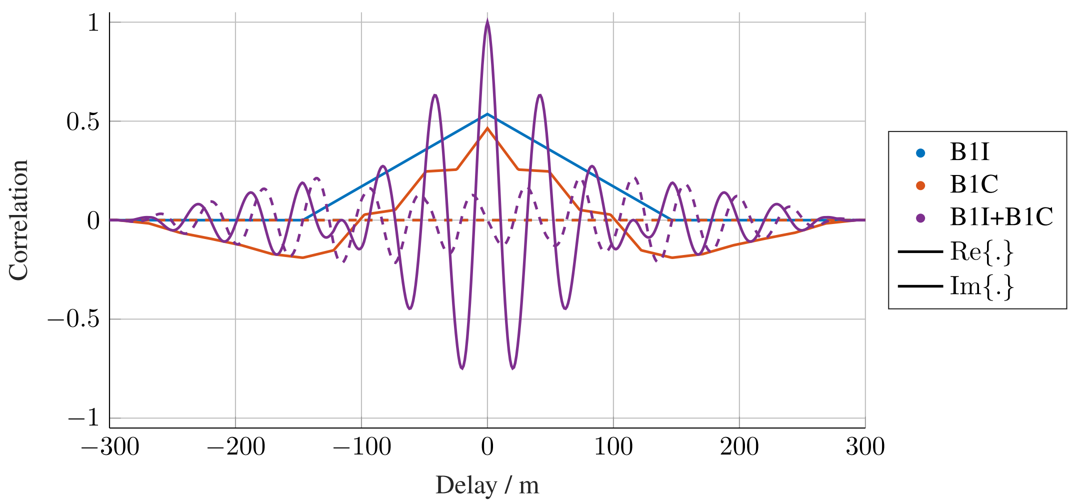

Figure 2: *BDS-3 B1 Signal auto-correlation functions*

The joint use of multiple GNSS stand-alone signals with a given frequency offset can be achieved by dual band tracking (DBT) and MSP, where DBT techniques are a subset of MSP strategies. In the early stages of the MSP discussion, simultaneous tracking of L- and S-band signals was investigated by Issler et al. (2010). Later, the ranging performance potential of meta-signals consisting of pre-existing signals in the lower L-band was discussed (Das et al., 2020; Ortega et al., 2020b,a; García-Molina, 2021). Due to the ongoing discussion regarding the introduction of "quasi-pilot" signals and in the context of low earth orbit (LEO) positioning, navigation and timing (PNT), proposals and general concepts for more narrowband meta-signals have been explored (Nardin et al., 2020a; Borio and Gioia, 2022; García-Molina et al., 2022; Beck et al., 2023).

A first study by Nardin et al. (2020b) investigated the effect of distortions on a MSP implementation. In general, a meta-signal ACF has an inherent ambiguity problem as it contains a sharp main peak, which theoretically enables a significant ranging performance boost, but has relatively high and stable side maxima, which, if misidentified as the main peak, can lead to significant pseudorange errors of several meters especially in low carrier-to-noise density ratio (C/N_0) regimes (Schwalm et al., 2020) and harsh propagation environments. Payload distortions can be the result of non-ideal components used in the signal generation chain, in particular during power amplification and filtering. The effect of payload distortions does not only affect meta-signals with a mere range bias, but leads to a more severely deformed cross-correlation function (CCF), resulting in an increased probability of incorrectly tracking side maxima of the CCF.

In this work, we assess the meta-signal time of arrival (TOA) tracking performance degradation due to payload distortions, assuming a set of representative linear and nonlinear distortions. As for meta-signal processing schemes, we assume a DBT implementation proposed by Wang et al. (2017) as well as a wideband MSP implementation to assess the expected performance degradation. The performance of the investigated meta-signal is reported in terms of TOA root-mean-squared error (RMSE) and jitter for different C/N_0 and different payload deformation scenarios by executing Monte Carlo simulations, adding colored noise in the post-correlation domain. We illustrate the interaction of non-linear and linear payload distortions and identify that linear payload distortion is the main cause of ranging accuracy degradation for more realistic payload assumptions.

II. SYSTEM MODEL

The following section describes the complete system model in baseband representation, which will be used later for the performance evaluation.

1. Transmitter and Channel

The first part of the GNSS signal propagation chain includes the transmitter and channel comprising an input multiplexer (IMUX), a high power amplifier (HPA), an output multiplexer (OMUX), and the channel, assuming only path loss and propagation delay as illustrated by Fig. 3 where $c_1(t)$ and $c_2(t)$ denote the B1I and B1C spreading waveform respectively, and $\mathbb{M}$ denotes the multiplexing function. The baseband payload model generates the BDS 3$^{\text{rd}}$ generation (BDS-3) B1 signals such that the (legacy)

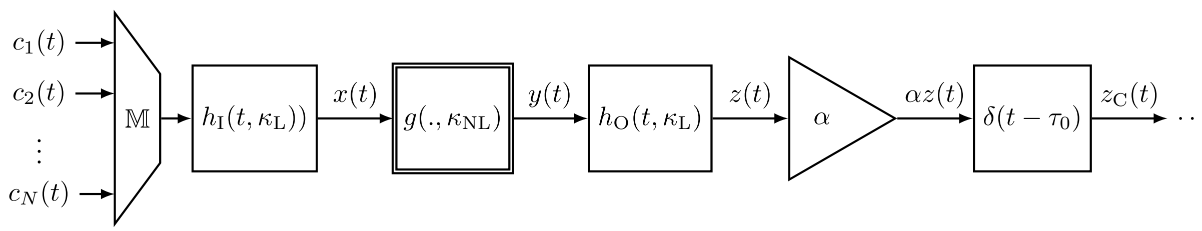

Figure 3: *Baseband Model of Satellite Transmitter and Channel*

B1I signal (China Satellite Navigation Office, 2019) and the B1C signal (China Satellite Navigation Office, 2017) attain the frequency offset of $f_\mathrm{meta} = 1/T_\mathrm{meta} \triangleq f_{0,\mathrm{H}} - f_{0,\mathrm{L}} = f_{0,\mathrm{B1C}} - f_{0,\mathrm{B1I}} = 14.322$ MHz and the frequency center is in middle of the carrier frequencies of the stand-alone civil signals. Consequently, the sub-carrier frequency of the BDS B1I+B1C signal is defined as $f_\mathrm{sub} = f_\mathrm{meta}/2 = 7.161$ MHz.

The special feature of this payload model is its configurability in terms of distortion by introducing the $\kappa_\mathrm{NL} \in [0,1]$ and $\kappa_\mathrm{L} \in [0,1]$ parameters. Setting the distortion parameters close to 0 means simulating the payload with minimal distortion, while setting them close to 1 simulates the payload with realistic distortion. κ_NL is the non-linear distortion parameter that controls the HPA only and κ_L is the linear distortion parameter that controls the IMUX and OMUX distortion simultaneously.

The memoryless HPA model with scalable distortion is based on five separate memoryless HPA models characterized with their input amplitude to output amplitude (AM/AM) and input amplitude to output phase (AM/PM) functions. The scalable distortion is achieved by morphing an idealized model with infinite output power backoff (OBO) and a small-signal gain of 15.97 dB, a hard-limiter model with the same gain but an OBO of 3.0 dB at 30.00 dBm input power, a measured model with idealized pre-distortion, a measured model with realistic pre-distortion, and a measured model without pre-distortion using sinussoidal weights, as used in (Beck et al., 2023), between the models' AM/AM and AM/PM functions. For all HPA models at input power of 30.00 dBm the output power is 45.97 dBm.

The amplitude responses of the intermediate states of the scalable distortion model for the OMUX filter are shown in Fig. 4. The amplitude responses are modeled with a 6$^{\text{th}}$-order Butterworth characteristic centered at the B1C center frequency. Increasing the κ_L parameter reduces the bandwidth, resulting in moderate distortion. Note that the IMUX filter is modeled in the same way as the OMUX filter, but with much wider bandwidths. The two-sided 3-dB bandwidths of IMUX and OMUX intermediate filter models are reported by Tab. 1. For the IMUX filter, we assume an all-zero phase response in all distortion states. This is not the case for the OMUX. The OMUX filter is modeled with an all-zero phase response $\kappa_\mathrm{L} \leq 0.6$. For $\kappa_\mathrm{L} > 0.6$, the phase response is modeled to be non-zero, which results in the group delay shown in Fig. 5.

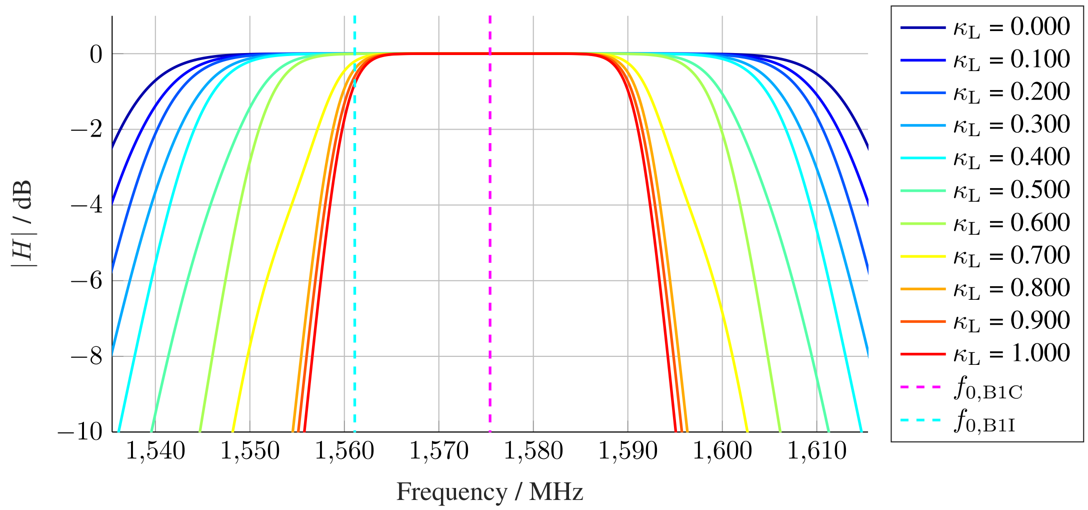

Figure 4: *Amplitude Response of Scalable OMUX Filter in Passband*

Table 1: *Two-sided 3-dB Bandwidths of the IMUX and OMUX Filters in MHz*

κ_L	0.00	0.20	0.40	0.60	0.80	1.00
IMUX	409.20	204.60	163.68	102.30	92.07	81.84
OMUX	81.840	73.656	65.472	51.150	34.782	32.736

2. Receiver

The latter part of the system model is the receiver side, of which two variants were investigated.

Notation

Both receiver models are presented in a vectorized notation such that the correlator outputs are computed $\boldsymbol{q}_n = \boldsymbol{C}_n^\mathrm{H}\boldsymbol{s}$ where $\boldsymbol{s} \in \mathbb{C}^{N_\mathrm{s}\times 1}$ denotes a sampled receive signal,

$$\boldsymbol{C}_n^{(i)} = \boldsymbol{C}_n(\hat{\tau}^{(i)} - \boldsymbol{\tau}_n) = \begin{bmatrix} c_n(\boldsymbol{t} - \hat{\tau}^{(i)} + \boldsymbol{\tau}_n(1)) & c_n(\boldsymbol{t} - \hat{\tau}^{(i)} + \boldsymbol{\tau}_n(2)) & \cdots & c_n(\boldsymbol{t} - \hat{\tau}^{(i)} + \boldsymbol{\tau}_n(N_\mathrm{c})) \end{bmatrix} \in \mathbb{C}^{N_\mathrm{s}\times N_\mathrm{c}} \tag{1}$$

the n-th correlator bank with N_c correlators in the i-th tracking loop iteration, and $\boldsymbol{t} \in \mathbb{R}^{N_\mathrm{s}\times 1}$ the query time vector of the replica. The entries of correlator output vector $\boldsymbol{q}_n$ correspond to the individual very-early (VE), early (E), prompt (P), late (L), and very-late (VL) correlator outputs such that

$$\mathrm{Re}\{\boldsymbol{q}_n\} = [I_\mathrm{E} \quad I_\mathrm{P} \quad I_\mathrm{L}]^\mathrm{T} \tag{2a}$$

$$\mathrm{Im}\{\boldsymbol{q}_n\} = [Q_\mathrm{E} \quad Q_\mathrm{P} \quad Q_\mathrm{L}]^\mathrm{T} \tag{2b}$$

if $N_\mathrm{c} = 3$ or

$$\mathrm{Re}\{\boldsymbol{q}_n\} = [I_\mathrm{VE} \quad I_\mathrm{E} \quad I_\mathrm{P} \quad I_\mathrm{L} \quad I_\mathrm{VL}]^\mathrm{T} \tag{3a}$$

$$\mathrm{Im}\{\boldsymbol{q}_n\} = [Q_\mathrm{VE} \quad Q_\mathrm{E} \quad Q_\mathrm{P} \quad Q_\mathrm{L} \quad Q_\mathrm{VL}]^\mathrm{T} \tag{3b}$$

if $N_\mathrm{c} = 5$.

DBT receiver

The first receiver is a DBT implementation featuring only one brick-wall front-end filter centered at 0 MHz and with a two-sided front-end receiver bandwidth $B_\mathrm{FE} = 24.552$ MHz. The DBT receiver then shifts the signal by ± 7.161 MHz such that the B1I and B1C signal can be independently correlated in their baseband with their respective correlator bank using front-end filter-matched replicas. Fig. 6 shows the DBT receiver model.

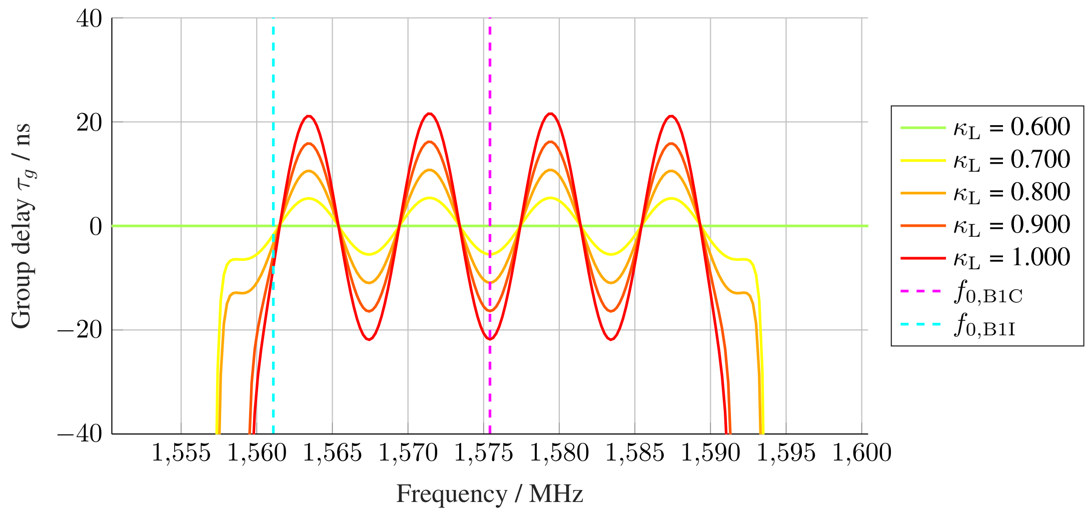

Figure 5: *Group Delay of Scalable OMUX Filter in Passband*

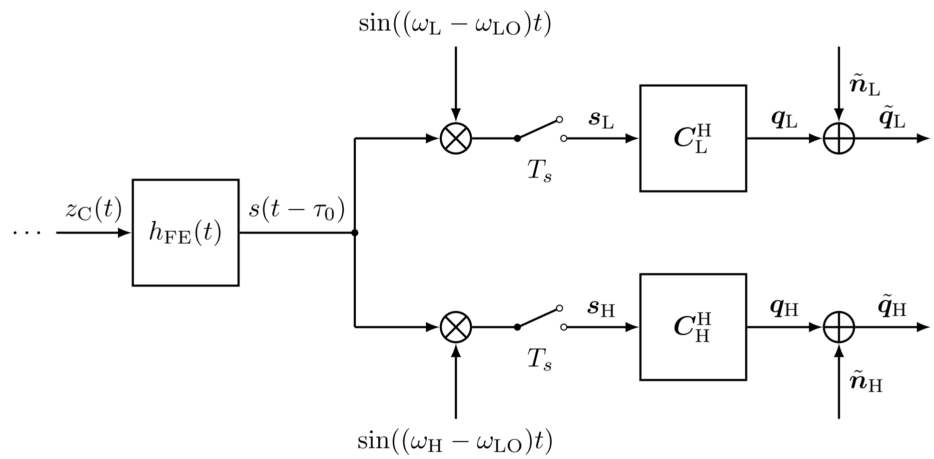

Figure 6: *Noise-Equivalent Baseband Model of DBT Receiver*

Wideband MSP receiver

The second receiver is a wideband MSP receiver that processes the BDS B1I+B1C signal as a composite signal by correlating with a composite complex replica $c_m(t) = c_1(t)e^{-2\pi f_{sub} t} + c_2(t)e^{+2\pi f_{sub} t}$. Hence, the correlation of the MSP receiver is performed by only one correlator bank. For a fair comparison, we use the same front-end filter as for the DBT receiver. Fig. 7 shows the MSP receiver model. In both models, colored noise is applied to the correlator outputs using a coloring matrix based on the front-end receiver bandwidth and the correlator banks. This approach yields noise-equivalent receiver models enabling a faster Monte Carlo simulation as used by Beck et al. (2023). The B1I correlator bank $\boldsymbol{C}_L \in \mathbb{R}^{N_s \times 3}$, B1C correlator bank $\boldsymbol{C}_H \in \mathbb{R}^{N_s \times 5}$, and the B1I+B1C correlator bank $\boldsymbol{C}_M \in \mathbb{C}^{N_s \times 5}$ are updated for each tracking loop iteration and attain the correlator spacings

$$\boldsymbol{\tau}_{B1I} = [-\Delta_{1,B1I}/2 \quad 0 \quad +\Delta_{1,B1I}/2]^T \, T_{c,B1I} \tag{4a}$$

$$\boldsymbol{\tau}_{B1C} = [-\Delta_{2,B1C}/2 \quad -\Delta_{1,B1C}/2 \quad 0 \quad +\Delta_{1,B1C}/2 \quad +\Delta_{2,B1C}/2]^T \, T_{c,B1C} \tag{4b}$$

$$\boldsymbol{\tau}_{meta} = [-\Delta_{2,meta}/2 \quad -\Delta_{1,meta}/2 \quad 0 \quad +\Delta_{1,meta}/2 \quad +\Delta_{2,meta}/2]^T \, T_{meta} \tag{4c}$$

with $\Delta_{1,B1I} = 1.00$, $\Delta_{1,B1C} = 0.50$, $\Delta_{2,B1C} = 1.00$, $\Delta_{1,meta} = 0.50$, $\Delta_{2,meta} = 1.92$, and $T_{c,n}$ denoting the chipping frequency of the n-th waveform.

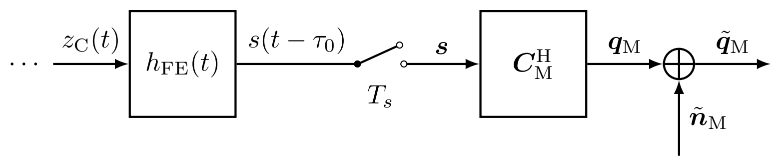

Figure 7: *Noise-Equivalent Baseband Model of MSP Receiver*

S-Curves

A generic set of coherent early-late processing (CELP) and non-coherent early-late processing (NELP) discriminators for the DBT and MSP receiver may be defined as

$$d_{\mathrm{coh,DBT}}(\hat{\tau}) = \gamma_{\mathrm{coh,DBT}} \left(\gamma_{\mathrm{L}} \frac{I_{\mathrm{E,L}} - I_{\mathrm{L,L}}}{I_{\mathrm{P,L}}} + \gamma_{\mathrm{H}} \frac{I_{\mathrm{E,H}} - I_{\mathrm{L,H}}}{I_{\mathrm{P,H}}} \right) \tag{5a}$$

$$d_{\mathrm{non,DBT}}(\hat{\tau}) = \gamma_{\mathrm{non,DBT}} \left(\gamma_{\mathrm{L}} \frac{I_{\mathrm{E,L}}^2 + Q_{\mathrm{E,L}}^2 - I_{\mathrm{L,L}}^2 - Q_{\mathrm{L,L}}^2}{I_{\mathrm{E,L}}^2 + Q_{\mathrm{E,L}}^2 + I_{\mathrm{L,L}}^2 + Q_{\mathrm{L,L}}^2} + \gamma_{\mathrm{H}} \frac{I_{\mathrm{E,H}}^2 + Q_{\mathrm{E,H}}^2 - I_{\mathrm{L,H}}^2 - Q_{\mathrm{L,H}}^2}{I_{\mathrm{E,H}}^2 + Q_{\mathrm{E,H}}^2 + I_{\mathrm{L,H}}^2 + Q_{\mathrm{L,H}}^2} \right) \tag{5b}$$

$$d_{\mathrm{coh,MSP}}(\hat{\tau}) = \gamma_{\mathrm{coh,MSP}} \frac{I_{\mathrm{E,M}} - I_{\mathrm{L,M}}}{I_{\mathrm{P,M}}} \tag{5c}$$

$$d_{\mathrm{non,MSP}}(\hat{\tau}) = \gamma_{\mathrm{non,MSP}} \frac{I_{\mathrm{E,M}}^2 + Q_{\mathrm{E,M}}^2 - I_{\mathrm{L,M}}^2 - Q_{\mathrm{L,M}}^2}{I_{\mathrm{E,M}}^2 + Q_{\mathrm{E,M}}^2 + I_{\mathrm{L,M}}^2 + Q_{\mathrm{L,M}}^2} \tag{5d}$$

where Eq. 5a and Eq. 5c is CELP and Eq. 5b and Eq. 5d is NELP (Wang et al., 2017). Hereby only the early (E), prompt (P) and late (L) correlator outputs are used for the code-delay discrimination. The very-early (VE) and very-late (VL) correlator outputs are only implemented for the detection of tracking a false lock point. The discriminator gains γ are chosen such that we have a linear relationship of the true signal delay and the discriminator output in a neighborhood around the correct delay-locked loop (DLL) lock point. Applying the chosen correlator spacings, the DLL discriminator or "S-curves" can be evaluated, which is shown in Fig. 8. Each positively-sloped zero crossing constitutes a stable tracking point of the DLL. DBT has a wide pull-in

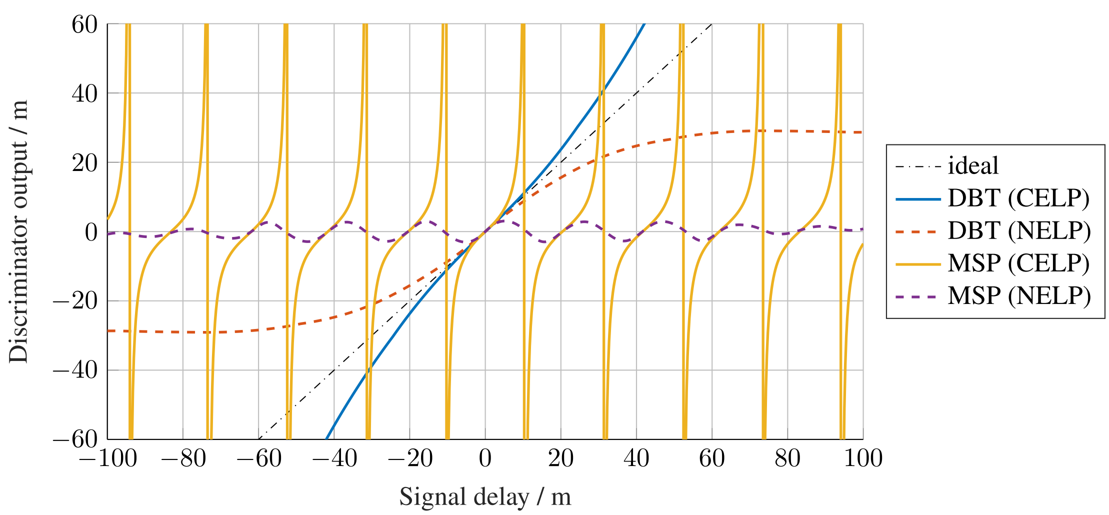

Figure 8: *S-Curves of DBT and MSP DLL Discriminators*

range for the one and only stable attraction point. The MSP receiver, on the other hand, has multiple stable points of attraction, only one of which is the correct lock point. When using the DBT, a slightly incorrect initialization of the tracking loop would eventually result in the correct signal delay. When using the MSP, the code-delay ambiguity problem is choosing the correct lock point. Therefore, an MSP receiver must then implement a code-delay ambiguity strategy such as bump jumping (Fine and Wilson, 1999) to eventually arrive at the tracking interval of the correct lock point.

Tracking loop

We use a first order tracking loop with TOA estimate update rule

$$\hat{\tau}^{(i+1)} = s_0\, d(\hat{\tau}^{(i)}) + \hat{\tau}^{(i)} + \hat{e}_{\text{jump}}(\hat{\tau}^{(i)})\, t_{\text{jump}} \tag{6}$$

where $e_{\text{jump}} \in \{-1, 0, +1\}$ denotes the jumping direction and t_{jump} the respective bump jumping time offset. The one-sided DLL bandwidth is $B_{\text{DLL}} = 10.0$ Hz and the choice of the parameter $\omega_0 = B_{\text{DLL}}/4 = 2.5$ Hz results in $s_0 = \omega_0\, T_{\text{int}} = 0.025$ (Kaplan and Hegarty, 2005) when assuming an integration time of $T_{\text{int}} = 10$ ms. The bump jump implementation evaluates the bump jump direction estimates

$$e_{\text{jump}} = \begin{cases} -1 & I_{\text{VL}}^2 + Q_{\text{VL}}^2 > I_{\text{P}}^2 + Q_{\text{P}}^2 \wedge I_{\text{P}}^2 + Q_{\text{P}}^2 > I_{\text{VE}}^2 + Q_{\text{VE}}^2 \\ +1 & I_{\text{VL}}^2 + Q_{\text{VL}}^2 < I_{\text{P}}^2 + Q_{\text{P}}^2 \wedge I_{\text{P}}^2 + Q_{\text{P}}^2 < I_{\text{VE}}^2 + Q_{\text{VE}}^2 \\ 0 & \text{else} \end{cases} \tag{7}$$

and accumulates the current and last 19 jump estimates to the applied bump jump direction estimate

$$\hat{e}_{\text{jump}}(\hat{\tau}^{(i)}) = \text{round}\left(\frac{1}{20} \sum_{k=i-19}^{i} e_{\text{jump}}(\hat{\tau}^{(k)})\right) \tag{8}$$

by computing a sliding mean. After a bump jump invocation, bump-jumping disabled until 20 new jump estimates have been collected.

III. PERFORMANCE MEASURES

Our main performance measures in the ranging perfromnace evaluation is the steady state tracking TOA estimation RMSE

$$\text{RMSE}_n = \sqrt{\frac{1}{N_{\text{MC}}} \sum_{n_{\text{MC}}=1}^{N_{\text{MC}}} \left(\tau_n^{(n_{\text{MC}})} - \tau_0\right)^2} \tag{9}$$

and the steady state tracking TOA estimation jitter

$$\sigma_n = \sqrt{\frac{1}{N_{\text{MC}}} \sum_{n_{\text{MC}}=1}^{N_{\text{MC}}} \left(\tau_n^{(n_{\text{MC}})} - \tau_{\text{bias}} - \tau_0\right)^2} \tag{10}$$

where N_{MC} denotes the total number of Monte Carlo experiments, $\tau_n^{(n_{\text{MC}})}$ denotes the n_{MC}-th Monte Carlo realization of a TOA estimate, and τ_{bias} denotes the TOA estimation bias which is derived from a noise-free realization for each evaluated $(\kappa_{\text{NL}}, \kappa_{\text{L}})$ tuple.

IV. NUMERICAL RESULTS

This section reports the numerical results of the conducted case study. As in Wang et al. (2017), we assumed a signal power ratio for generation $P_{\text{B1C}}/P_{\text{B1I}} = 3/4 = -1.2494$ dB. This study shows the results for NELP only when using an integration time of $T_{\text{int}} = 10$ ms. The RMSE and jitter are based on $120,000$ Monte-Carlo tracking loop estimates in steady state for each payload configuration with a randomized true signal delay τ_0.

1. Steady state tracking RMSE with scalable distortion payload

The evaluation of the steady-state tracking RMSE for the DBT and MSP receiver models, using the introduced scalable distortion payloads, is discussed below.

Thermal noise performance in extreme case

Fig. 9 shows the steady-state tracking RMSE for the DBT and MSP receiver. In the medium and high C/N_0 regimes, the RMSE of MSP is on average ten times smaller than that of DBT. In a low C/N_0 regime, MSP loses its performance advantage and enters the threshold region due to the ambiguity problem as explored for general signals by Weiss and Weinstein (1983). For

DBT and MSP, the increased variance and bias introduced by the payload leads to an early saturation of the RMSE at around 32.5 dB-Hz for the more distorted payload scenarios.

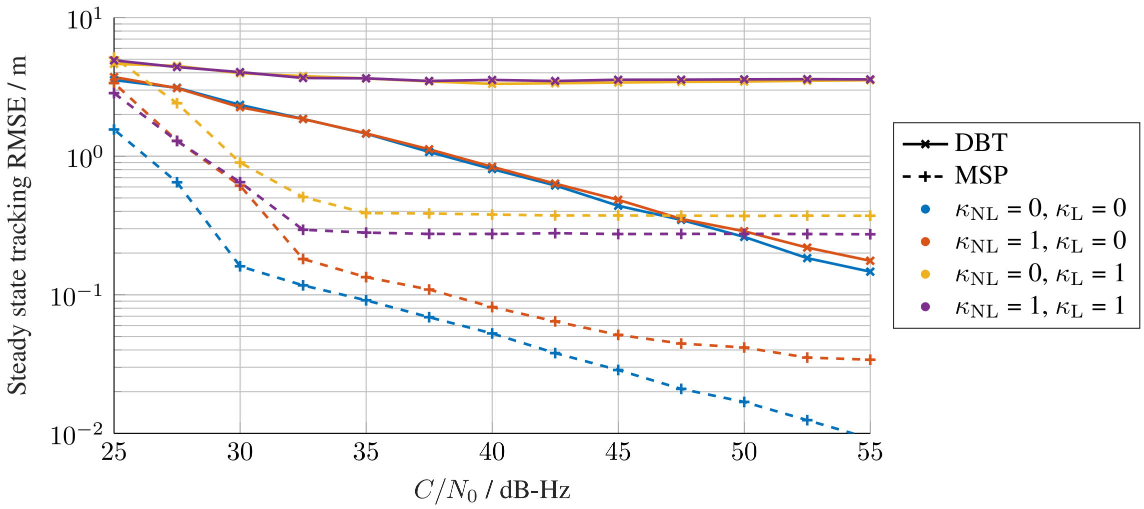

Figure 9: *Steady State Tracking RMSE of DBT and MSP in Extreme Cases of Payload Distortion*

Thermal noise performance at 40 dB-Hz

The interaction of non-linear and linear distortions on the steady-state tracking RMSE for a C/N_0 of 40 dB-Hz is shown by Fig. 10 and Fig. 11 for DBT and MSP respectively. For DBT, the influence of linear distortion is greater than of non-linear distortion. The impact of non-linear distortion grows only slightly with increasing linear distortion, which is consistent with our previous observations. As seen earlier, the RMSE of MSP is ten times lower than that of the DBT. Similar to the DBT, the influence of linear distortions is greater than that of non-linear distortions. However, we observe a stronger influence of non-linear distortions on the MSP than on the DBT receiver.

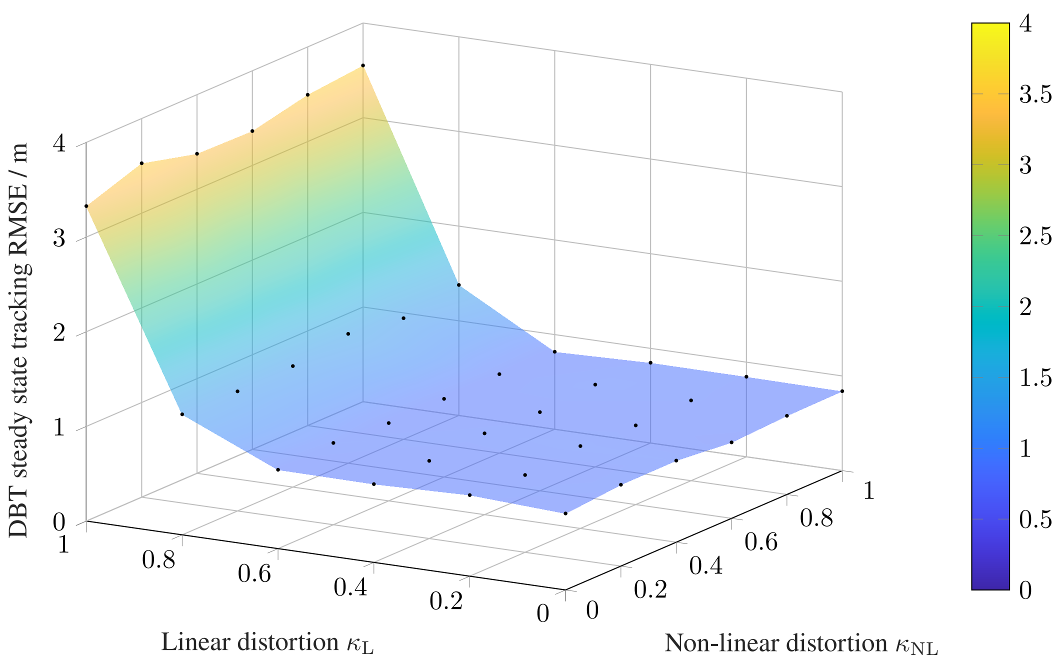

Figure 10: *DBT Steady State Tracking RMSE at* 40.0 *dB-Hz*

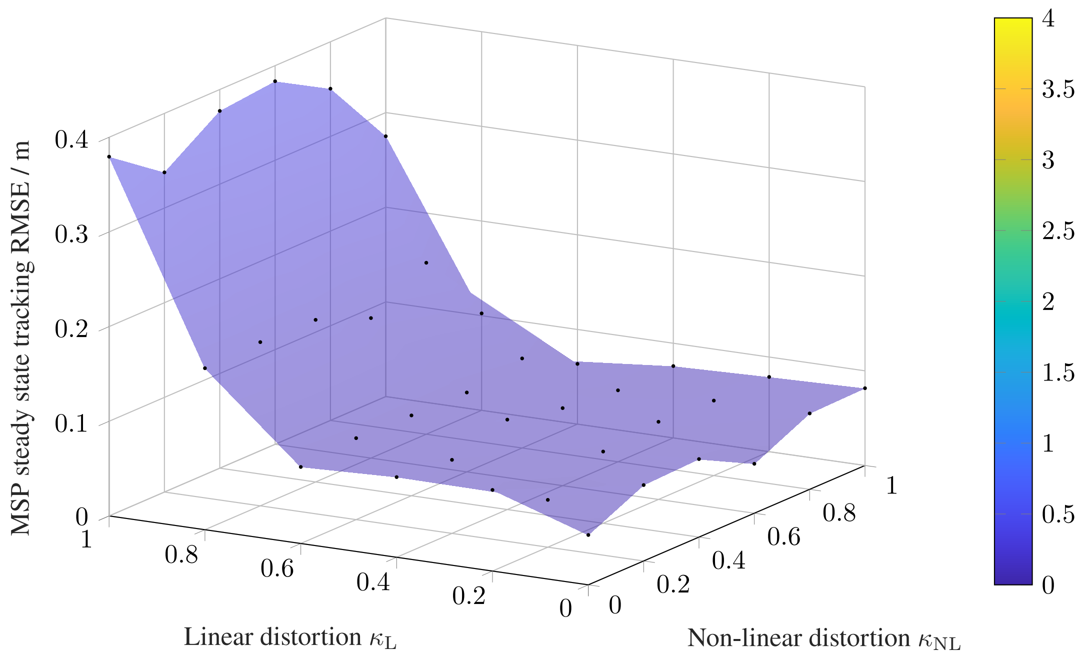

Figure 11: *MSP Steady State Tracking RMSE at* 40.0 *dB-Hz*

2. Steady state tracking jitter with scalable distortion payload

The evaluation of the steady-state tracking jitter for the DBT and MSP receiver models, using the introduced scalable distortion payloads, is discussed below.

Fig. 12 shows the steady-state tracking jitter for the DBT and MSP receiver. A first observation is that the DBT suffers less

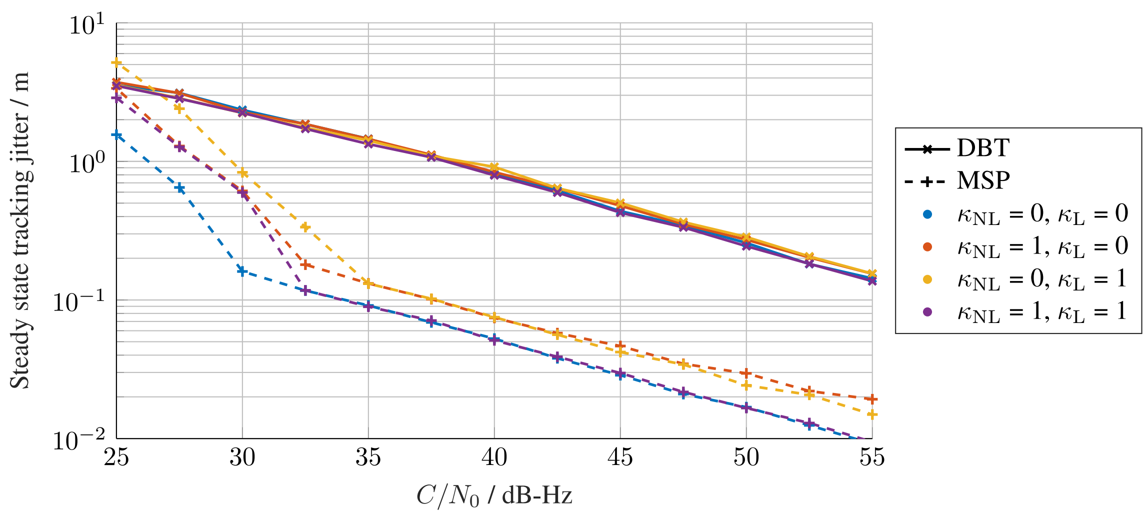

Figure 12: *Steady State Tracking Jitter of DBT and MSP in Extreme Cases of Payload Distortion*

from variance introduced by payload distortion at different distortion states. It appears that the tracking jitter is independent of the distortion level, which allows us to conclude that the bias is the primary source of error for the DBT approach in a realistic payload scenario. However, the tracking jitter of MSP shows a dependence on the distortion level, resulting in ranging performance degradation, constituting a "distortion gap" as explored by Beck et al. (2023), that reflects the increased variance due to the asymmetry of the CCF. The evaluated multiplicative MSP "distortion gap" is approximately 1.65, meaning that the payload distortion affected the estimation process such that the TOA jitter is systematically increased even with knowledge of the bias.

V. CONCLUSION

DBT and MSP strategies are key to improving signal performance in terms of ranging accuracy for users of signals within the upper L-band, as it is unlikely that new wideband stand-alone signals will be made available to civil users in the foreseeable future. However, it may be more likely that certain GNSS operators will choose to surgically place new narrowband signals in spectral gaps for emerging user needs. Therefore, a preliminary evaluation of DBT and MSP strategies has been conducted to assess the impact of non-linear and linear payload distortion on meta-signal ranging performance.

Based on the presented case study of the BDS B1I+B1C meta-signal, linear payload distortion was identified as the primary cause of the degradation in ranging accuracy. The effect of non-linear payload distortion increases as linear distortion increases. Wideband MSP may be feasible for realistic payload scenarios if distortions are mitigated while operating in the medium to high C/N_0 range. When distortions are considered, the probability of losing a correct lock increases and the ambiguity problem is exacerbated.

Future research should investigate channel effects such as ionospheric delay and multipath. A study of the impact of payload distortions on the BDS B1I+B1C signal with measured BDS-3 payload imperfections on DBT and MSP strategies is open work.

ACKNOWLEDGMENTS

This work has been carried out within the framework of the projects HiGAIN and CySNAB within the German Aerospace Center (DLR).

REFERENCES

Anghileri, M., Floch, J. J., Margaria, D., Motella, B., Peña, A. G., Julien, O., Macabiau, C., Chauvat, R., and Paonni, M. (2018). FUNTIMES–Future Navigation and Timing Evolved Signals. In *Proc. of the 31st International Technical Meeting of the Satellite Division of The Institute of Navigation (ION GNSS+ 2018)*, pages 876–912.

Beck, F. C., Enneking, C., Thölert, S., and Meurer, M. (2023). Galileo Performance Improvements employing Meta-Signals – Robustness Analysis against Payload and Receiver Distortions. European Navigation Conference 2023.

Betz, J. W. and Kolodziejski, K. R. (2009). Generalized Theory of Code Tracking with an Early-Late Discriminator Part I: Lower Bound and Coherent Processing. *IEEE Transactions on Aerospace and Electronic Systems*, 45(4):1538–1556.

Borio, D. and Gioia, C. (2022). GNSS Meta-signals, Dual-Frequency Combinations and the Double Phase Estimator. In *Proc. of the 2022 International Technical Meeting of The Institute of Navigation*, pages 1015–1026.

China Satellite Navigation Office (2017). BeiDou Navigation Satellite System Signal In Space Interface Control Document Open Service Signal B1C (Version 1.0). http://en.beidou.gov.cn/SYSTEMS/ICD/201806/P020180608519640359959.pdf (Retrieved: 2023-07-07).

China Satellite Navigation Office (2019). BeiDou Navigation Satellite System Signal In Space Interface Control Document Open Service Signal B1I (Version 3.0). http://en.beidou.gov.cn/SYSTEMS/ICD/201902/P020190227702348791891.pdf (Retrieved: 2023-07-07).

Das, P., Ortega, L., Vilà-Valls, J., Vincent, F., Chaumette, E., and Davain, L. (2020). Performance Limits of GNSS Code-Based Precise Positioning: GPS, Galileo & Meta-Signals. *Sensors*, 20(8):2196.

Fine, P. and Wilson, W. (1999). Tracking Algorithm for GPS Offset Carrier Signals. In *Proceedings of the 1999 National Technical Meeting of The Institute of Navigation*, pages 671–676.

García-Molina, J. A. (2021). Unambiguous Meta-Signal Processing. *Inside GNSS*.

García-Molina, J. A., Wallner, S., Vazquez, C., De Pasquale, G., Del Peral-Rosado, J. A., Da Broi, G., Schmitt, T., Melman, F., Parro, J. M., Soualle, F., Flochs, J. J., and Lopez-Risueno, G. (2022). Quasi-Pilot Signals: Acquisition and Fast Time Ambiguity Resolution. In *2022 10th Workshop on Satellite Navigation Technology (NAVITEC)*.

Issler, J.-L., Paonni, M., and Eissfeller, B. (2010). Toward centimetric positioning thanks to L-and S-Band GNSS and to meta-GNSS signals. In *2010 5th ESA Workshop on Satellite Navigation Technologies and European Workshop on GNSS Signals and Signal Processing (NAVITEC)*, pages 1–8. IEEE.

Kaplan, E. D. and Hegarty, C. J. (2005). *Understanding GPS Principles and Applications*. ARTECH HOUSE, INC., 685 Canton Street, Norwood, MA 02062, USA, second edition edition.

Nardin, A., Dovis, F., and Fraire, J. A. (2020a). Empowering the Tracking Performance of LEO PNT by Means of Meta-Signals. In *2020 IEEE International Conference on Wireless for Space and Extreme Environments (WiSEE)*, pages 153–158. IEEE.

Nardin, A., Dovis, F., and Motella, B. (2020b). Impact of non-idealities on GNSS meta-signals processing. In *2020 European Navigation Conference (ENC)*, pages 1–8. IEEE.

Ortega, L., Medina, D., Vilà-Valls, J., Vincent, F., and Chaumette, E. (2020a). Positioning Performance Limits of GNSS Meta-Signals and HO-BOC Signals. *Sensors*, 20(12):3586.

Ortega, L., Vilà-Valls, J., Chaumette, E., and Vincent, F. (2020b). On the Time-Delay Estimation Accuracy Limit of GNSS Meta-Signals. In *2020 IEEE 23rd International Conference on Intelligent Transportation Systems (ITSC)*, pages 1–6. IEEE.

Paonni, M. and Bavaro, M. (2013). On the Design of a GNSS Acquisition Aiding Signal. In *Proc. of the 26th International Technical Meeting of The Satellite Division of the Institute of Navigation (ION GNSS+ 2013)*, pages 1445–1456.

Schwalm, C., Enneking, C., and Thölert, S. (2020). Ziv-Zakai Bound and Multicorrelator Compression for a Galileo E1 Meta-Signal. In *2020 European Navigation Conference (ENC)*, pages 1–9. IEEE.

Sénant, E., Gadat, B., Charbonnieras, C., Roche, S., Aubault, M., and Marmet, F.-X. (2018). Tentative New Signals and Services in Upper L1 and S Bands for Galileo Evolutions. In *Proc. of the 31st International Technical Meeting of The Satellite Division of the Institute of Navigation (ION GNSS+ 2018)*. Institute of Navigation.

Wang, C., Cui, X., Ma, T., Zhao, S., and Lu, M. (2017). Asymmetric Dual-Band Tracking Technique for Optimal Joint Processing of BDS B1I and B1C Signals. *Sensors*, 17(10):2360.

Weiss, A. and Weinstein, E. (1983). Fundamental limitations in passive time delay estimation–Part I: Narrow-band systems. *IEEE Transactions on Acoustics, Speech, and Signal Processing*, 31(2):472–486.